Optimization of an Aircraft Wing

Team 6:
Jacob Maneth, Bret Wainwright, Peter Harper

May, 2016
MAE 598 – Design Optimization

Author Contributions

Jacob Maneth

- Content of Subsections 1.3, 2.2, 3.2, 4.2, 5.2, 5.3, 6.2, and 7.2
- Content of Section 8
- Approach and theory behind modal analysis subsystem optimization
- Approach, implementation, and execution of ANSYS simulations for all subsystems

Bret Wainwright

- Content of Subsections 1.2, 2.1, 3.1, 4.1, 5.1, 6.1, and 7.1
- Approach and theory behind aerodynamics subsystem optimization

Peter Harper

- Content of Subsections 1.4, 2.3, 3.3, 4.3, 5.4, 6.3, and 7.3
- Approach and theory behind deflection subsystem optimization

Abstract

This design project will focus on the optimization of an aircraft wing for a specific cruise speed and cruise angle of attack. The process for optimizing the wing will start with adjusting the shape of a standard NACA airfoil. The pressure distribution on the airfoil will be calculated and then used for a topology optimization of the internal structure of the airfoil. The resulting airfoil and internal structure will be extruded to create a three-dimensional wing which will undergo analysis to determine the wing's deflection and modal response. The results of the wing deflection and modal response will be used to adjust the internal structure with the goal of minimizing the deflection and maximizing the first modal response.

Identifying an optimal airfoil shape for use in an aircraft wing for a certain cruise speed and angle of attack can allow savings in weight and improvements in safety and reliability. These in turn can lead to financial savings for companies that operate the aircraft due to reduced fuel consumption and lower maintenance costs. Weight savings allows for less material to be used and leads to a design that is more efficient. Reduced fuel consumption means that there are fewer emissions, which results in a cleaner environment.

Table of Contents

Table of Figures

Table of Tables

1. Design Problem Statement

1.1. Introduction

This design project will focus on the optimization of an aircraft wing for a certain cruise speed and cruise angle of attack. The process for optimizing the wing will be done by varying the shape of the airfoil and internal structure of the wing to minimize weight and drag and maximizing the first order modal response of the wing. An example of a tradeoff in this project is between weight and the first order modal response. One method to maximize the first order modal response of a wing is to increase the amount of material used. However, increasing the material used means the wing weight increases and goes against the goal to minimize weight. While there has been a lot of work done in the area of optimizing airfoils, optimizing both the shape and internal structure is unique to this project.

For the purposes of this project the problem of wing optimization has been broken down into three subsystems or areas of focus which are: aerodynamics, modal response, and deflection. As noted earlier, there are tradeoffs that must be considered in this project. The shape of the airfoil can increase or decrease the drag and pressure. If the pressure on the wing increases, then the internal structure must be stronger and will most likely require more material. Additional material can improve the first order modal response, but it detracts from the goal to minimize the weight of the wing. Deflection might also benefit from additional material, but again this takes away from the goal to minimize weight. The three subsystems can initially be setup and run independently, but they must be integrated early on. This is due to the many tradeoffs that arise as one factor is changed and how it influences the other factors.

1.2. Subsystem 1 – Aerodynamics

The aerodynamics subsystem is a major precursor for the other two subsystems. The shape of an aircraft's airfoil greatly affects the performance of the aircraft and needs to be carefully shaped for both aerodynamic and structural considerations. The design of an airfoil plays a major role in allowing an aircraft to perform at its cruise point. The airfoil is crucial for determining the lift an aircraft's wing can generate, how fast it can efficiently fly, and how much pressure drag is created by the wing (which affects the thrust required for the aircraft). At the same time, the airfoil must be structurally sound and needs to be able to operate at high loading conditions. It also should be stable in the pitch axis and should not have an exceedingly negative pitching moment.

When designing the shape of the airfoil, the primary trade-off will be between the lift generated and wave drag caused by shockwaves forming on the airfoil. Once shocks begin to form on the airfoil, the overall drag of the airfoil will increase

greatly. The Mach number at which shocks begin to form (critical Mach number) is primarily dependent on the minimum pressure on the upper surface of the airfoil. However, lower minimum pressures also generally result in more lift. The maximum thickness of the airfoil also plays a role in determining the critical Mach number (thinner airfoils have higher critical Mach numbers), but this is obviously constrained by structural concerns. Both the minimum pressure and the thickness of the airfoil should be considering when looking at the results from the airfoil optimization.

In the design of an aircraft, the cruise condition is the most important condition, so the airfoil should be optimized for this scenario. The cruise point of an aircraft is defined by the aircraft's altitude, flight Mach number, weight (required lift), and required thrust. Considering a specific speed and payload are generally a goal for an aircraft, it would make sense to optimize for minimum drag which is directly related to the amount of thrust the aircraft requires. As such, this subsystem will be optimized for minimum drag with an equality constraint for lift and an inequality constraint for moment. Since this problem is primarily concerned with the design of the airfoil, the wing of the aircraft will be assumed to have a constant sweep, chord, and no taper ratio. This gives a constant lift distribution over the span of the wing while excluding 3D effects which are irrelevant to the airfoil's analysis. Ultimately, everything relates back to the z-coordinates of the airfoil, which will be optimized at set spacing along the chord of the airfoil.

Much research has already been done on the optimization of airfoils for cruise performance. Most optimization studies have been done for a specific aircraft or set of conditions. Generally, a new airfoil needs to be optimized for a different set of conditions, so the design task is still valid. Very few studies also attempt to optimize the internal structure of the airfoil as well, so this aspect of the optimization is relatively unique. A similar type of optimization was done by Marc Drela in his paper *Pros and Cons of Airfoil Optimization* (Drela, 1998), and it provides good insight into how to approach this problem.

1.3. Subsystem 2 – Modal Response

The subsystem being optimized is the internal structure of a wing. The objective is to maximize the first modal response of the structure, so as to reduce the likelihood of aerodynamic flutter occurring. This will be achieved by varying the thickness of several internal spars, with the tradeoff being the weight of the wing. It is expected that in order to increase the first modal response of the wing, more material will be used, thereby increasing the weight of the wing.

Real wings are designed to prevent flutter, and so there is a great body of prior work available. One paper of interest was written by Vivek Mukhopadhyay of NASA's Langley Research Center and is titled *A Conceptual Wing Flutter Analysis Tool for Systems Analysis and Parametric Design Study*. In this paper, the author presents an interactive way of conducting flutter analysis. One main conclusion that can be drawn from the paper is that the wing-root chord torsional stiffness is a key factor in designing a flutter-free wing. Therefore, maximizing the first modal response may be achieved by increasing the torsional stiffness of the wing.

1.4. Subsystem 3 – Deflection

As with the modal response subsystem, the subsystem being optimized is the internal structure of a wing. The objective for the deflection subsystem is to maintain the deflection of the wing to within a reasonable range. Using the same method as the modal response subsystem, thickness of several internal spars will be varied to minimize weight while also maintaining the structural integrity of the wing.

2. Nomenclature

2.1. Aerodynamics

Name		Description	Units
M_{des}	=	design Mach number	
M_{crit}	=	critical Mach number	
W	=	weight	[lbs]
C_L	=	lift coefficient	
C_l	=	sectional lift coefficient	
C_d	=	sectional drag coefficient	
C_P	=	pressure coefficient	
C_m	=	moment coefficient	
q	=	dynamic pressure	[psi]
ρ	=	density	[slugs/ft^3]
c	=	chord	[ft]
b	=	span	[ft]
Alt	=	altitude	[ft]
u	=	flow velocity	[ft/s]
g	=	body accelerations	[ft/s^2]
P	=	pressure	[psi]
v	=	kinematic viscosity	[ft^2/s]
S_{ref}	=	reference area	[ft^2]
x_c	=	X position as a fraction of total chord length	
z_c	=	Z position as a fraction of total chord length	
F_x	=	sectional forces in the x direction	[lbf/ft]
F_z	=	sectional forces in the z direction	[lbf/ft]
Cf_x	=	coefficient of Fx	
Cf_z	=	coefficient of Fz	
$\propto$	=	angle of attack	
Λ	=	sweep angle	

2.2. Modal Response

Name		Description	Units
t_{skin}	=	skin thickness	[in]
t_i	=	thickness of the i^{th} spar	[in]
w	=	overall system weight	[lbs]
u	=	displacement matrix	[in]
M	=	mass matrix	[lbs]
C	=	damping matrix	[lbf-sec/in]
K	=	stiffness matrix	[lbs/in]
F	=	force matrix	[lbf]
ω_i	=	i^{th} natural frequency of the system	[Hz]
$[\dot{\ }]$	=	1st time derivative of a variable	
$[\ddot{\ }]$	=	2nd time derivative of a variable	

2.3. Deflection

Name		Description	Units
u_i	=	deflection of the i^{th} spar	[in]
u	=	displacement matrix	[in]

3. Mathematical Model

3.1. Aerodynamics

3.1.1. Objective Function

As previously mentioned, the objective is to minimize the sectional drag of the airfoil by changing the z_c coordinates of the airfoil. The computation to get sectional drag from an airfoil shape is quite complex. ANSYS Fluent will be used to do the computational fluid dynamics necessary to solve the Navier-Stokes equation (Anderson, 2003) over the airfoil:

$$\frac{\partial \boldsymbol{u}}{\partial t} + \boldsymbol{u} \cdot \nabla \boldsymbol{u} = -\frac{1}{\rho}\nabla \bar{P} + \upsilon \nabla^2 \boldsymbol{u} + \frac{1}{3}\upsilon \nabla(\nabla \cdot \boldsymbol{u}) + \boldsymbol{g} \tag{1}$$

ANSYS Fluent will give the pressure distributions over the airfoils as an output. By integrating this pressure distribution over the upper and lower surfaces, the forces in the x and z directions (F_x, F_z) can be found. Then by using trigonometry and the given angle of attack for the airfoil, the sectional lift and sectional drag coefficients can be calculated.

$$C_{fx} = \int C_P dz \tag{2}$$

$$C_{fz} = \int -C_p dx \tag{3}$$

$$C_l = C_{f_z}\cos(\alpha) - C_{f_x}\sin(\alpha) \tag{4}$$

$$C_d = C_{f_z}\sin(\alpha) + C_{f_x}\cos(\alpha) \tag{5}$$

Therefore, the drag of the airfoil will be minimized by adjusting the z_c coordinates of the airfoil. The objective function is then:

$$\min C_d = f(z_c) \tag{6}$$

3.1.2. Constraints

The primary equality constraint necessary for this optimization problem is on how much lift the airfoil needs to generate. To meet the lift requirement, a necessary C_l value needs to be calculated. For the purpose of this optimization problem, an aircraft with the following specifications will be used:

Altitude	=	35000ft
M_{des}	=	0.8
c	=	15ft
b	=	100ft
W	=	20000lbs
Λ	=	35°
$\propto$	=	1.5°

The first step is to find the dynamic pressure at this altitude and cruise Mach number (0.8). This can easily be found on a standard atmosphere table and it has a value of 223.71 psf.

The required C_l value can then be calculated with the following equation because the wing has a constant twist, taper, and chord.

$$C_l = \frac{W}{q * c * b} = 0.6 \tag{7}$$

So the C_l value calculated by ANSYS needs to be equal to or greater than 0.6.

Additionally, based on previous experiments (Drela, 1998) a constraint needs to be included regarding the moment coefficient of the airfoil. Logically this makes sense, because the optimizer will likely try to create higher pressures in the rear of the airfoil, creating a strong negative moment. This would require the aircraft to have heavy and powerful trim tabs to counter the moment. Without knowing more about the airfoil, a guess of a minimum C_m of -0.13 about the quarter chord seems reasonable. The following equation can be used to calculate C_m from the pressure data given by ANSYS.

$$C_m = \int (x - 0.25) * C_P dx + \int z * C_P dz \tag{8}$$

The remaining constraints that need to be imposed involve geometric constraints on the airfoil itself. The airfoil will consist of 8 points on the upper surface of the airfoil and 8 points on the lower surface. These points will be restricted to specific x_c positions, and these locations will be focused primarily to the front and rear of

the airfoil. The leading and trailing edges will be fixed at $x_c = 0$ and $z_c = 0$, and $x_c = 1$ and $z_c = 0$, respectively. The leading edge needs to remain blunt, so the angle will be constrained to be 180°. Obviously, constraints will also exist that prevent the upper surface and lower surface from intersecting. This can be written as z_c for the upper surface can never be less than z_c for the lower surface.

Additionally, there needs to be a limit on maximum and minimum thickness. Based on other existing airfoils, a logical maximum for thickness should be about 15% and a minimum should be approximately 3%. Each point on the upper and lower surfaces needs to have unique upper and lower limits on its possible values of z_c. These bounds were determined based on other existing airfoils and by looking at the maximum and minimum possible airfoil shapes. As different random airfoils were generated during the optimization, some issues such as the upper and lower splines intersecting began to arise. When this occurred, the geometric boundary conditions were updated to avoid this issue all together. As such, these boundaries went through many changes throughout the course of the project until the final geometric boundaries were found. These bounds are shown in Table 3-1.

Table 3-1 Upper and Lower Bounds of Control Points

	X Position (in)	Lower Bound – Z (in)	Upper Bound – Z (in)	Range (in)
Upper Surface	3.969172	19.23	23.7	4.47
	16.55925	22.18	27.99	5.81
	62.04228	25.54	31.41	5.87
	90.10566	25.1	31.41	6.31
	118.0195	23.89	29.7	5.81
	143.1121	21.05	24.2	3.15
	162.9513	19.25	20.93	1.68
	175.6481	16.1	16.8	0.7
Tail	180	15	15	0
Lower Surface	175.6481	14.06	15	0.94
	162.9513	11.99	15	3.01
	143.1121	9.93	15	5.07
	118.0195	5.98	15	9.02
	90.10566	4.41	15	10.59
	62.04228	4.41	15	10.59
	16.55925	5.68	14.58	8.9
	3.969172	7.29	14.53	7.24

3.1.3. Design Variables and Parameters

The design variables and parameters for the aerodynamic subsystem are fairly simple. The airfoil will have 8 control points per surface, with fixed leading and trailing edges. Each control point will have a fixed x_c coordinate and can only move vertically in the z_c direction. This gives each control point a single degree of freedom, resulting in 16 degrees of freedom total. Sixteen was chosen because there is a large jump in the number of design points in ANSYS if more than 17 degrees of freedom are used, and 16 gives an equal number of points on the upper and lower surfaces. Additionally, since splines were being used to connect the points, using too many points could cause strange impossible geometries in the solution due to the complex fitting that is occurring.

There are a lot different airfoils that can be chosen and a significant portion of them could meet the constraints. An example of an airfoil that generally meets the constraints is the RAE-2822 supercritical airfoil, which research shows generates less lift and has lower drag. This airfoil will be tested in ANSYS to compare to the optimized airfoil. Coordinate data for the RAE-2822 airfoil (Slater, 2016) is available in Appendix A, along with an image of the airfoil.

3.1.4. Summary of Model

The problem is to design an airfoil shape using 16 control points around an airfoil to meet given cruise requirements including lift and drag. The pressure distribution around the airfoil will be solved for using the Navier-Stokes equation through the computation fluid dynamics medium of ANSYS Fluent. This pressure distribution can then be used to solve for the lift, drag, and moment coefficients of the airfoil. The process will be repeated a total of 289 times to create a fractional factorial design of experiments dataset that can be used to create a response surface. This response surface will then be optimized to find an airfoil with a minimum value of drag that meets the lift constraint. The airfoil also must meet structural constraints.

Objective: $\min C_d = f(z_c)$

Constraints:	$-C_l(z_c) + 0.6 \leq 0$	(Lift constraint)
	$-C_m(z_c) - 0.13 \leq 0$	(Moment constraint)
	$z_{c,i}(x_{c,i}) - UB(x_{c,i}) \leq 0$	(Geometric Upper)
	$-z_{c,i}(x_{c,i}) + LB(x_{c,i}) \leq 0$	(Geometric Lower)
	$\left(z_{cu}(x_{c,i}) - z_{cl}(x_{c,i})\right)_{max} - 0.15 \leq 0$	(Maximum Thickness)
	$\left(-z_{cu}(x_{c,i}) + z_{cl}(x_{c,i})\right)_{min} + 0.03 \leq 0$	(Minimum Thickness)
	$\theta_{LE} - 180° = 0$	(Leading Edge Angle)

3.2. Modal Response

3.2.1. Objective Function

Vibrations in a structure are not always a problem, but when those vibrations occur at a natural frequency of the structure they can be destructive. As was mentioned before, the objective of this subsystem optimization is to maximize the first modal response of a wing. This will be achieved by varying the thickness of several parts of the internal structure, while also aiming to keep the weight of the wing low.

The general-purpose finite element software ANSYS Mechanical will be used to perform the modal analysis and optimization of the structure. In general, a continuous structure has an infinite number of degrees of freedom (DOFs). A structure such as this is governed by the following equation of motion:

$$\boldsymbol{M\ddot{u} + C\dot{u} + Ku = F} \tag{9}$$

The finite element method approximates the continuous structure by using a fixed number of elements, thereby creating a fixed number of degrees of freedom (Herrin, 2012). Finding the natural frequencies and mode shapes is then just a matter of finding the eigenvalues and eigenvectors of the system in the above equation. The default method that ANSYS uses is the Block Lanczos method, which is ideal for large systems. The mass, damping, and stiffness matrices are all functions of the internal structure being optimized, and this internal structure is modified by changing the thickness of various parts. Therefore, the objective may be stated as:

$$\max \omega_1 = f(t_1, t_2, \dots, t_i) \tag{10}$$

3.2.2. Constraints

The constraints for this objective are primarily stated as upper and lower bounds on the thicknesses of the internal structure. These may be stated generally as:

$$t_{lower} \leq t_i \leq t_{upper} \tag{11}$$

Weight will be constrained by an inequality, with the maximum allowable weight for a single wing being 12000 lbs.

$$w \leq 12000\ lbs \tag{12}$$

By optimizing the first modal response, the maximum weight will likely be reached, and so the inequality constraint may become an equality constraint (the constraint will be active).

3.2.3. Design Variables and Parameters

The variables that will be used to optimize the internal wing structure will be the thickness of each internal spar, t_i. For this design, the skin thickness will be fixed at 0.125 in. and there will be a total of 16 spars. The spars will be positioned according to a shape optimization performed in ANSYS, which is shown in Section 5. The thickness of each of these spars will be allowed to vary continuously from 0.25 in. to 1 in.

3.2.4. Summary of Model

Objective: $\max \omega_1 = f(t_1, t_2, \dots, t_i)$

Constraints: $0.25\ in \leq t_i \leq 1.00\ in$

$w \leq 12000\ lbs$

3.3. Deflection

3.3.1. Objective Function

As with the modal response subsystem, the subsystem being optimized here is the internal structure of a wing. The objective is to minimize the deflection of the wing. Using the same method as the modal response subsystem, the thickness of sixteen internal spars will be varied to minimize weight while also maintaining the structural integrity of the wing. The objective may be stated as:

$$\min u = f(t_1, t_2, \dots, t_i) \tag{13}$$

3.3.2. Constraints

The constraints for this subsystem of the wing will be the same as those used for the modal response subsystem.

3.3.3. Design Variables and Parameters

The design variables for this subsystem of the wing will be the same as those used for the modal response subsystem.

3.3.4. Summary of Model

Objective: $\min u = f(t_1, t_2, \dots, t_i)$

Constraints: $0.25\ in \leq t_i \leq 1.00\ in$

$w \leq 12000\ lbs$

4. Model Analysis

4.1. Aerodynamics

Monotonicity analysis is not really viable for reducing the optimization problem, because the problem uses an extremely complicated simulation. It can be assumed that geometric constraints bound the vertical positions of each control point well, because there is one constraint below and one constraint above. Additionally, the goal of minimizing C_d and the constraint on C_l are opposing each other due to shock wave formation on the airfoil. This means the lift and the drag should also properly bound each other. As such, it can be said that the problem is well bounded.

In preliminary testing it was determined that too many control points would adversely affect the splines used to connect the points. This caused strange splines and the possibility of intersecting in some configurations. Originally, the trailing edge was allowed a small amount of vertical motion, but it was changed to be fixed. This was enough to resolve these issues, and this resulted in a simpler system with only 16 degrees of freedom as opposed to the initial 17. Additionally, the x-coordinates of the control points were shifted to allow for the creation of smoother splines with the upper and lower boundaries of z_c.

Right off the bat, it is not apparent which constraints will be active. In general however, the C_l constraint opposes the goal of minimizing C_d, so it is likely that the C_l constraint will end up being active. It is also possible that lift will not be a constraining factor of the optimization if the lift required is quite low. The idea is that if the required lift is small and easy to accomplish at the flight conditions, it may not be the determining factor in minimizing drag.

It should also be noted that because of an airfoil design's dependence on its flight conditions (angle of attack and incoming Mach number), generalizing the optimization model for variable conditions is not very useful. This is partly because of the great care that needs to be taken in creating the mesh for use in ANSYS Fluent.

4.2. Modal Response

Due to the complexity of the system being optimized, conventional tools such as monotonicity analysis could not be used to reduce the size of the optimization problem. This meant that the thickness range for each of the spars was selected so that none of the thickness constraints would become active. The reason for choosing such ranges was so that a global type of solution could be found, i.e. the best possible solution without being limited by constraints. With this approach, the only constraint that may become active would be the weight limit for a single wing.

Modeling of the wing utilized a simplified representation of the geometry. Originally, the skin thickness was also going to be allowed to vary. This caused difficulty in consistently obtaining valid geometry in ANSYS, so the thickness was fixed at 0.125 in. Furthermore, the analysis was simplified by modeling each of the spars and the skin as surfaces. This led to a greatly reduced number of elements and nodes in the model, which allowed for each simulation to be solved in under a minute. The model analyzed is shown in Figure 4-1.

Figure 4-1 Model of Airfoil Interior

4.3. Deflection

The subsystem being optimized was the deflection of a wing, and it was performed using ANSYS. There is only general information about what equations are being used. Detailed information about what algorithms are used and how the algorithms process the user inputs is not available. ANSYS then is basically a black box that receives inputs and then provides outputs. This means that monotonicity analysis or other basic methods for reducing the number of constraints or determining which constraints are active is not feasible.

The simplified representation of the wing geometry that was used for the modal response was also used for the deflection analysis. The simplifications with regard to fixing the skin thickness and modeling each spar and the skin as surfaces were also incorporated.

5. Optimization Study

5.1. Aerodynamics

The actual optimization of the airfoil was also done using ANSYS, and the setup in ANSYS is shown in Appendix B. Even though multiple Response Surface Optimizations were tested, the “Genetic Aggregation” optimization method was used to analyze the design space and find the optimal solution. The benefit of using Genetic Aggregation is that the algorithm tries out multiple response surfaces, and then uses a fitness function to determine the best response surface. The “best” response surface is defined by both its accuracy and its stability in the fitness function. Genetic Aggregation can either select a single best response surface, or it can patch together multiple response surfaces that are the best in different regions. The optimal solution is then solved for from the response surface using “Non-Linear Programming by Quadratic Lagrangian”, which is a sequential quadratic programming method.

The optimal solution found is shown in Figure 5-1, and its data points as compared to the upper and lower bounds are shown in Table 5-1.

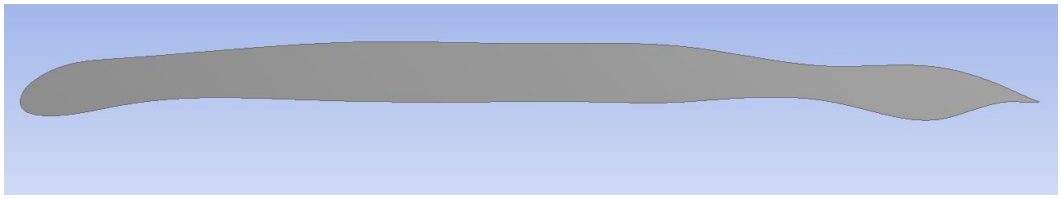

Figure 5-1 Optimized Airfoil Shape

Table 5-1 Optimized Airfoil Coordinates

	X Position (in)	Lower Bound-Y (in)	Upper Bound-Y (in)	Optimized Design (in)
Upper Surface	3.969172	19.23	23.7	19.6988
	16.55925	22.18	27.99	22.5336
	62.04228	25.54	31.41	25.54
	90.10566	25.1	31.41	25.2004
	118.0195	23.89	29.7	24.5939
	143.1121	21.05	24.2	21.234
	162.9513	19.25	20.93	20.93
	175.6481	16.1	16.8	16.8
Tail	180	15	15	15
Lower Surface	175.6481	14.06	15	15
	162.9513	11.99	15	11.99
	143.1121	9.93	15	15
	118.0195	5.98	15	15
	90.10566	4.41	15	15
	62.04228	4.41	15	15
	16.55925	5.68	14.58	14.14
	3.969172	7.29	14.53	12.57

Looking at the airfoil coordinates in the table, there were quite a few points on the airfoil that hit the upper boundary defined by the geometric constraints. This means that these constraints ended up being active for this problem. However, this information may not be as useful as it seems because the same airfoil could practically be generated by shifting all coordinates down by 2 inches. It does indicate however that the airfoil was being pushed to have higher and higher camber. Additionally, it brings into question whether or not the upper boundary conditions were high enough. From a practical standpoint, these upper bounds could not be pushed much higher because the highly cambered airfoils that could be generated would become exceedingly difficult to build structurally. Another constraint could be added to try to accommodate these structural considerations, but it would likely be difficult to implement without doing structural analysis.

Table 5-2 shows the aerodynamic data for the optimized airfoil compared to the constraints. It is easy to see that all of the aerodynamic constraints are met by the optimized airfoil. In particular, it is interesting to note that the C_l of the optimized airfoil is much higher than that which is required. This means the C_l constraint was not active, contrary to expectation. To uncover the reasons behind this, a detailed analysis of the optimized airfoil will be done in the results section of this report.

Table 5-2 Aerodynamic Data for the Optimized Airfoil

Objective / Constraints		Optimized Airfoil
Drag coefficient, Cd	minimize	0.04468429
Lift Coefficient, Cl	≥ 0.6	0.64845996
Moment Coefficient, Cm	≥ -0.13	-0.10165086

One benefit of using the genetic aggregation method is that it is relatively independent of the initial guess. It also follows that the optimal solution found is close to, if not the, global solution to the problem presented. This, however, does not mean this is a perfectly optimized airfoil; any issues with the methodology of the model itself will cause the solution found to diverge from the actual optimal solution for the given flight conditions. Potential sources of such errors will be discussed in the discussion and results section, along with possible suggestions to remedy these errors in future airfoil optimization research.

5.2. Internal Shape Optimization

In order to get a baseline for the internal structure of the airfoil, a shape optimization was run using ANSYS. The optimized geometry of the airfoil was used as the basic shape, and the pressure data from Fluent was used for the loading. Two sets of boundary conditions were tested. The first of these applied the upper surface and lower surface pressure data to the airfoil and had the trailing and leading edges as fixed points. With the goal of an 80% area reduction, Figure 5-2 shows the resulting internal structure.

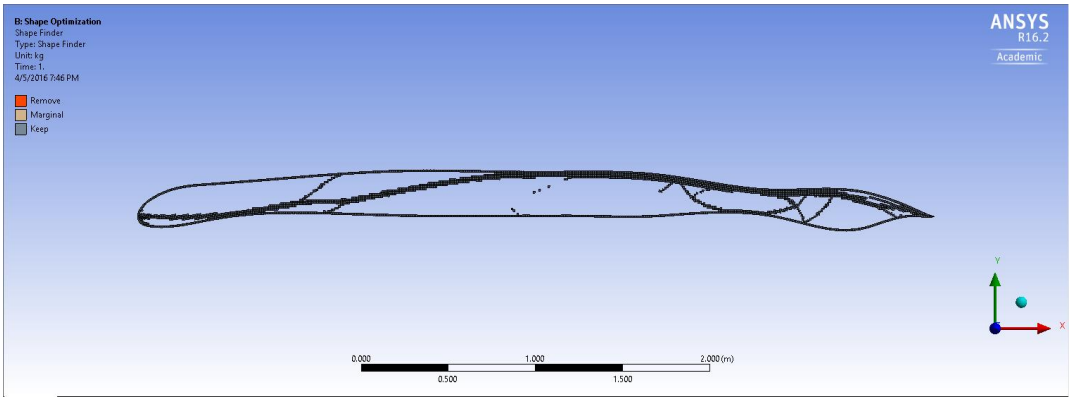

Figure 5-2 Fixed Leading/Trailing Edge Points

The second set of boundary conditions applied only the upper surface pressure data to the airfoil and it had the lower surface as being fixed. The same area reduction was used as before, and Figure 5-3 shows the resulting internal structure.

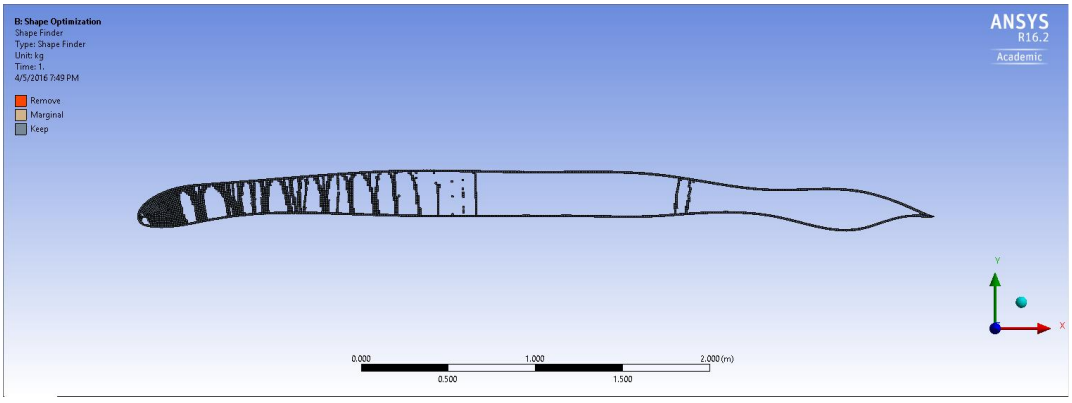

Figure 5-3 Fixed Lower Surface

From these two structures, it is obvious that the support conditions are important as they lead to dramatically different solutions. The internal structure in Figure 5-2 is conceptually interesting, but it is impractical to physically implement and control in the optimization due to the complicated geometry. Therefore, the

internal structure of Figure 5-3 was chosen as the baseline. This structure more closely resembles realistic wing structures, and it is much easier to model and control in the optimization process due to the multiple linear spar-like structures.

5.3. Modal Response

Optimization of the internal structure was carried out in ANSYS Mechanical using a response surface optimization approach. This method requires the use of a fractional factorial design of experiments (DoE). The DoE type selected was the Optimal Space-Filling Design (OSFD), which aims to equally space the generated design points in the design space. The advantage to using this DoE type over the other available types is that design points which are near neighbors are avoided, and so the entire design space is uniformly explored. A disadvantage, though, is that the number of required design points may be higher, causing the total simulation time to be higher, too.

Once the DoE matrix was generated and all of the design points solved for, a response surface could be generated. The default type is a Full 2nd Order Polynomials response surface. For this subsystem, this response surface fit the data very well, as can be seen below.

	P39 - Total Deformation Maximum	P57 - Geometry Mass	P75 - Total Deformation Reported Frequency
⊟ Coefficient of Determination (Best Value = 1)			
Learning Points	0.99997	1	0.99998
⊟ Root Mean Square Error (Best Value = 0)			
Learning Points	0.010973	0.31315	5.0086E-05
⊟ Relative Maximum Absolute Error (Best Value = 0%)			
Learning Points	1.6064	0.16659	2.4643
⊟ Relative Average Absolute Error (Best Value = 0%)			
Learning Points	0.44606	0.052391	0.2972

Figure 5-4 Full 2nd Order Polynomials Fit Data

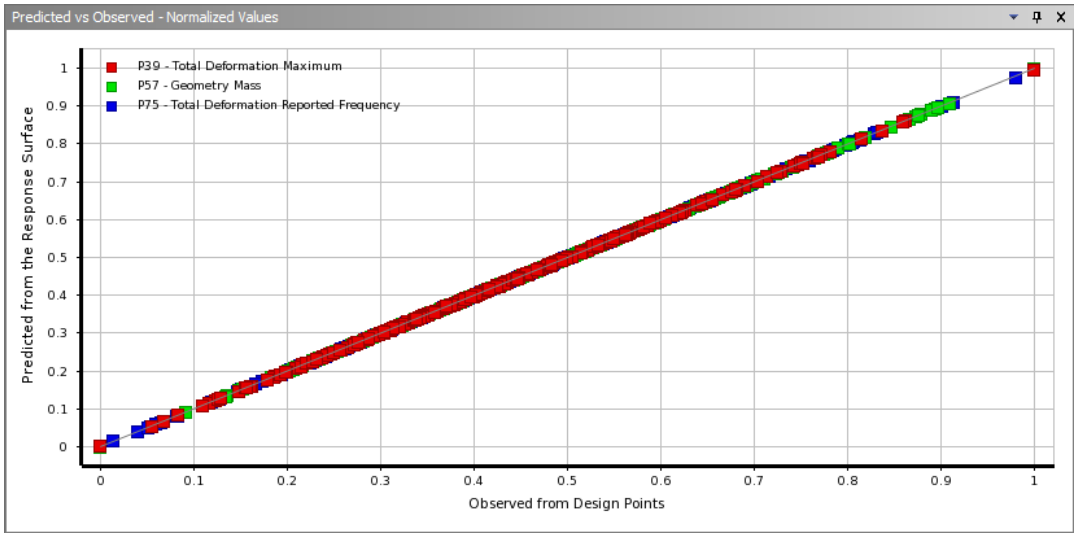

Figure 5-5 Predicted vs. Observed Values

In Figure 5-4 all relative errors are below 3%, which indicates a very good fit to the data; this is further seen in Figure 5-5.

To determine the optimal subsystem design, the Multi-Objective Genetic Algorithm (MOGA) was used. The objectives were to minimize deflection, to maximize the first modal response frequency, and to keep the weight of the wing below 12000 lbs. The optimizer was set to find three candidate points, which were then verified. The candidate selected was the one with minimal weight and maximum first modal response frequency. Figure 5-6 shows the optimized airfoil interior, and Table 5-3 shows the thickness of each of the spars. Table 5-4 shows the optimized values of the objectives.

Figure 5-6 Optimized Airfoil Interior

Table 5-3 Optimized Spar Thickness (Spars Numbered Left to Right)

Spar #	1	2	3	4	5	6	7	8
Thickness (in.)	0.837	0.610	0.619	0.656	0.715	0.394	0.391	0.961

Spar #	9	10	11	12	13	14	15	16
Thickness (in.)	0.655	0.941	0.809	0.616	0.902	0.730	0.849	0.326

Table 5-4 Optimized Objective Values

Objective		Optimized Value
Deflection	Minimize	64.444 in
Weight	≤ 12000 lbs	9066.2 lbs
1st Modal Frequency	Maximize	1.0873 Hz

From Table 5-3 it can be seen that this is an interior solution since none of the thickness constraints are active, although some are nearly active. This table also shows that the optimal solution is not to simply make all of the spars the same thickness, but rather certain areas of the structure need to be stiffer than others (i.e. thicker spars) in order to meet the objectives.

5.4. Deflection

As mentioned in the modal response section, a Multi-Objective Genetic Algorithm was used in ANSYS to find the optimal design for the following objectives: minimize deflection, maximize first modal response frequency and maintain the weight of the wing below 12,000 pounds. Based on the results from ANSYS, the optimal design was selected. The deflection values for the optimal design can be found in Table 5-4.

6. Parametric Study

6.1. Aerodynamics

In general, performing a parametric study on the aerodynamics of the airfoil and its optimization proves very difficult and sensitive. One reason for this is the long computational time of the CFD in the optimization. Additionally, the model and CFD is very sensitive to changes. This includes the airfoil shape, the constraints, and the flight conditions. The simulation being performed is extremely non-linear with respect to the upper and lower surface coordinates because, aerodynamically speaking, the exact airfoil coordinates do not have a very well defined effect on the pressure distribution of the airfoil. Extreme changes in flight conditions and the shape of the airfoil may also require the mesh to be remade which can greatly affect the convergence of the simulation.

In particular, though, changing the constraints that were found to be active as well as changing the flight conditions (especially incoming Mach number) could result in potentially very different optimal solutions. As a result it is not very feasible to try to generalize the results of this optimization. Each airfoil optimization problem must be carefully tailored to the conditions in which the airfoil will be used. Additionally, changing the boundaries of the airfoil geometry could result in sizeable changes in possible airfoil shapes due to the use of splines to connect the points together. If the boundaries are carefully tweaked, one could easily affect the type of airfoil produced by the optimization (such as the airfoil being thicker, thinner, more highly cambered, less highly cambered, more peaky in style, or more supercritical in style). The more freedom given to the vertical positions of the control points, the more types of airfoils the optimizer can find (both good and bad).

6.2. Modal Response

Due to the method used in optimizing the airfoil's interior structure, a parametric study would not prove to be useful. The OSFD DoE type makes it so that the initial starting point does not have a significant influence on the optimal solution. Furthermore, since none of the thickness constraints became active, a better solution would not be expected if the thickness constraints were expanded to cover a larger range.

The optimal solution is dependent on the airfoil shape, though, but changing the shape is not a possibility due to it already being the aerodynamically optimal shape for the given flight conditions. Because of this, the solution cannot be generalized any further than stating that the optimal solution is unlikely to have every spar at the same thickness. Thicker sections of the airfoil seem to require thicker spars, but this is not always the case as spars 6 and 7 are relatively thin compared to the neighboring spars.

6.3. Deflection

As discussed in the modal response section, the type of DoE used in optimizing the interior structure of the airfoil eliminated the need for a parametric study. In addition, since none of the thickness constraints are active and the airfoil shape itself is already optimized for the flight conditions, further efforts to improve the design beyond the current result would not yield better results.

7. Discussion of Results

7.1. Aerodynamics

The resulting airfoil from the optimization ended up being interesting to say the least. Visually, it displays characteristics from two different types of transonic airfoils: peaky airfoils (Pearcey, 1958) and supercritical airfoils (Harris, 1990). Peaky style airfoils tend have drooped leading edges, similar to the leading edge of the optimized airfoil. The idea behind this kind of airfoil is to have low pressures ahead of the maximum point on the upper surface of the airfoil (the airfoil's crest). Since the pressures act normal to the surface, the airfoil actually experiences "leading edge suction" which pulls the airfoil forward, countering some of the drag. In Pearcey's paper, this was mostly described as having a shock wave ahead of the crest to create a large pressure difference between the front and the back of the airfoil. However, as discussed briefly in *A Study of Conical Camber For Triangular and Sweptback Wing* (Boyd, 1955), this effect is also present, though in smaller quantities, for drooped airfoils without a shock near the leading edge because of the lift vector being angled forward.

Supercritical airfoils on the other hand try to push back the onset of drag divergence (shock formation) rather than reduce the drag caused by the shockwaves. This sort of airfoil, championed by Whitcomb, has a flat upper surface and usually has high camber at the trailing edge of the airfoil on the lower surface. The purpose of this kind of airfoil is to keep a large amount of the flow over the airfoil supersonic, with shock formation at the trailing edge after the airfoil's critical Mach number. This causes the pressure distribution of the airfoil to flatten, so that it does not hit the minimum pressure necessary to generate a shock wave until higher Mach numbers.

To make a better comparison to supercritical and peaky airfoils as well as to figure out what the airfoil is actually doing, analysis of the pressure distribution needs to be done. The pressure distribution on the surface of the airfoil can be seen in Figure 7-1, and the pressure field around the airfoil can be seen in Figure 7-2.

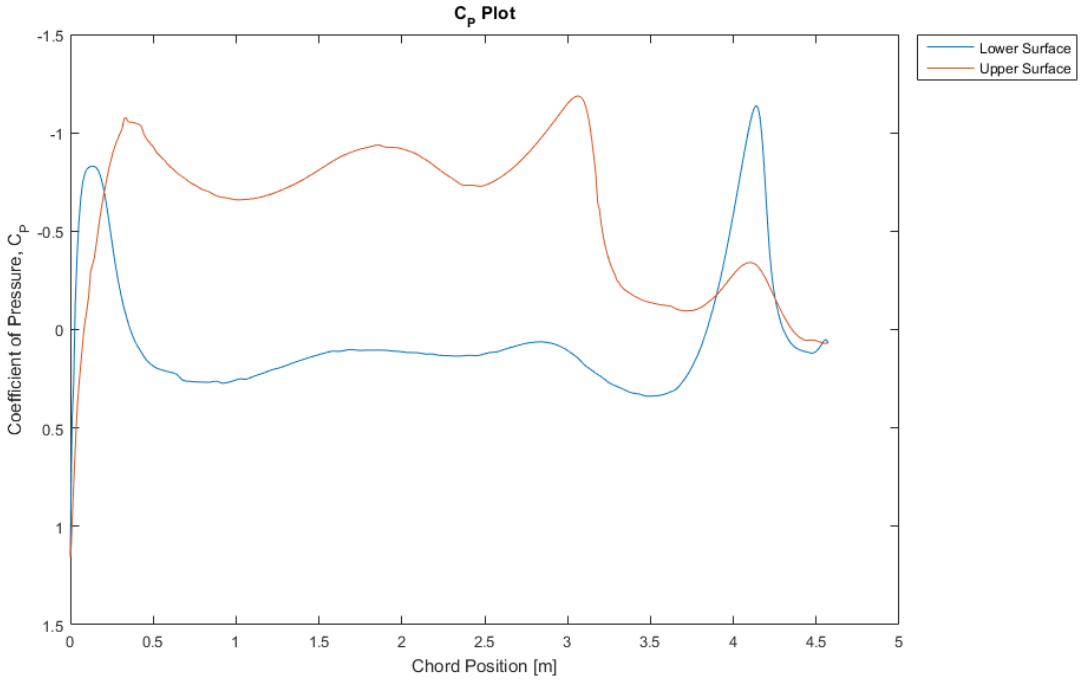

Figure 7-1 Pressure Distribution on the Airfoil Surface

This is the pressure distribution of the optimized airfoil. Note that on the y-axis positive C_P values are down and negative are up. The upper surface is in red and the lower surface is in blue.

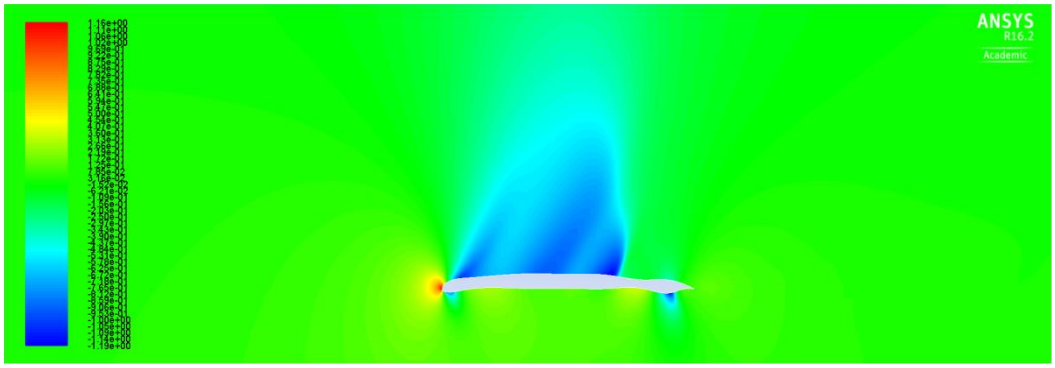

Figure 7-2 Pressure Field on the Optimized Airfoil

Blue areas represent low pressure. In general, the side of the airfoil with the low pressures is where the lift is being generated.

It is fairly evident from the pressure distribution that the shock wave is quite far back on the airfoil, with the pressure distribution being fairly flat. Consequently, this optimized airfoil is operating more like a supercritical airfoil rather than a peaky airfoil. In fact, based on the low pressure zone on the bottom of the airfoil's leading edge, the front of the airfoil is lifting downward slightly, which hurts the leading edge suction. The fluctuations in the pressure distributions are likely caused by the optimizer trying to find a flat topped airfoil, but due to the use of splines, the upper surface of the airfoil cannot be completely flat. It is interesting to note that the shockwave formed on the upper surface does not appear to be a strong one, as the pressure increase across the shock is slightly gradual rather than a flat drop. This lessens the energy losses across the shock and reduces drag slightly. The flat pressure distribution on this airfoil allows for the airfoil to generate more lift before a shock occurs.

Now to discuss the irregularity at the trailing edge of the airfoil: the lump. Few, if any, airfoils used outside of academia have this kind of lump at the trailing edge. Examining the pressure distribution, it appears to speed up the air on the lower surface which inevitably creates a fairly strong shock on the lower surface. It is evident from Figure 7-1 that this lump causes the airfoil to create negative lift on the trailing edge of the airfoil. So not only does this lump increase the wave drag on the airfoil, it also reduces the lift generated. The only benefit this lump incurs is that the airfoil will have a slightly smaller pitching moment. Though, because the moment constraint was not active during this optimization, it is very unlikely that the lump was created purposefully by the optimizer. As such, it was likely caused by an error or limitation in the model or airfoil generation method. In particular, it was probably caused by the use of splines to generate the airfoil. The trailing edge of the airfoil was forced to be a point, so the splines may have had to behave strangely to connect the ends and create a point. For example, if the last two points of the airfoil's coordinates were too close together in the X direction, the splines could become less smooth and misbehave in the region. In summary, the lump at the trailing edge was likely caused by a lack of freedom for the optimizer cause by the splines connecting the upper and lower surfaces. The optimizer likely was forced to try to make the best out of the model it was provided, creating an unavoidable, but optimal, lump at the trailing edge.

The next question regarding the optimal airfoil is "how well did it actually perform?" Is the airfoil actually a fairly good minimum drag solution? To determine this, the supercritical RAE-2822 airfoil was run through the same CFD setup to compare with the optimized solution. It is important to note that the flight Mach number used for this simulation is slightly greater than what a RAE-2822 is optimal for, but the results should still be comparable. Figure 7-3 shows the pressure distribution on its surface, Figure 7-4 shows the pressure field around the airfoil, and the Table 7-1 compares the aerodynamic results of the optimized airfoil to that of the RAE-2822.

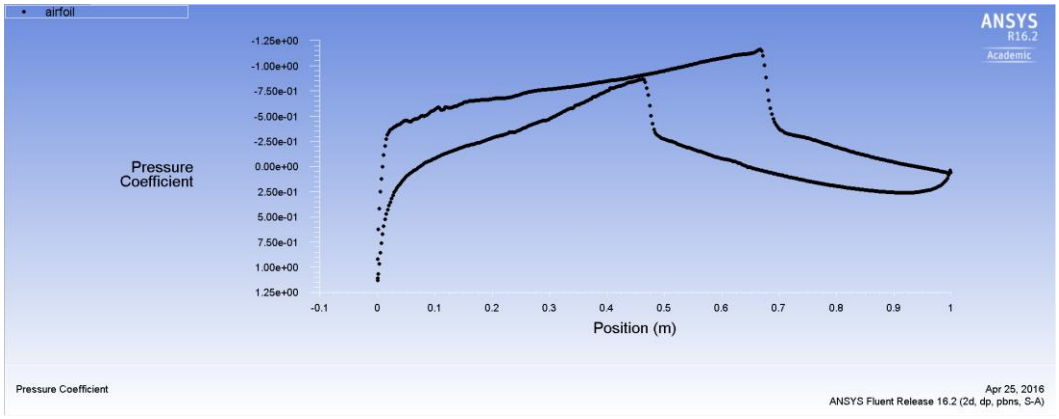

Figure 7-3 Pressure Distribution of RAE-2822

This is the pressure distribution of the RAE-2822. Note that this airfoil is normally flown at approximately Mach 0.76, not Mach 0.8. This is what causes the shock on the lower surface.

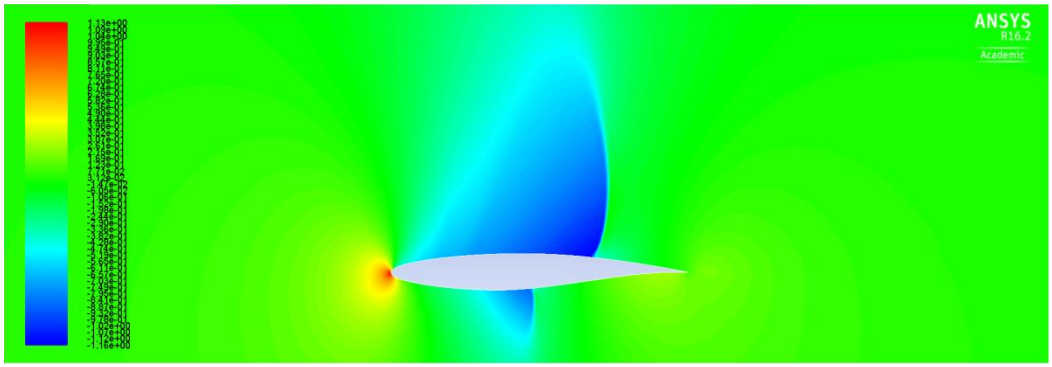

Figure 7-4 Pressure Field of RAE-2822

Blue areas represent low pressure. The shock on the lower surface reduces the pressure difference between the upper and lower surface, reducing lift.

Table 7-1 Comparison of Aerodynamic Data for RAE-2822

	RAE-2822	Optimized Airfoil
Drag coefficient, C_d	0.032679	0.044684
Lift Coefficient, C_l	0.4528	0.648459
Moment Coefficient, C_m	-0.111176	-0.10165

It is obvious that the optimized airfoil is probably better than the RAE-2822 at this flight condition. One major difference between the two is that the optimized airfoil generates significantly more lift for a marginal increase in drag. Considering that

the drag of an airfoil increases in a relatively parabolic fashion with increasing lift, the increase in the drag coefficient of 0.012 is not bad for an increase in the lift coefficient of 0.2.

If nothing else, the RAE-2822 simply does not generate enough lift to meet the necessary flight conditions. This reinforces the idea that every airfoil is usually designed for a single flight condition or aircraft, so the development of unique airfoils for specific conditions is useful. As such, it is difficult to directly compare the RAE-2822 airfoil with the optimized one, as they are designed for different conditions. Simplistically however, the RAE-2822 seems to generate disproportionately less lift for the amount of drag it has than the optimized airfoil. The optimized airfoil has a smaller in magnitude pitching moment than the RAE-2822 (though this is likely caused by the lump at the trailing edge), so it definitely seems that the optimized airfoil is a reasonable optimal solution to the design problem, though not perfect.

There are multiple ways that the optimization of the airfoil could potentially be improved in future research. The first improvement should be in the airfoil generation itself. In the current research, a lump was created at the trailing edge that hurt the airfoil's performance. There are a few ways this could be potentially be remedied. The simplest way to try to address this problem is to adjust the x coordinates of the control points to try to smooth out the splines at the trailing edge of the airfoil. This is likely not the best solution because tweaking the control point locations may not be able to prevent odd geometries altogether. A more general solution would be to increase the DoFs in the model and allow each control point to be moved horizontally. This would give the optimizer the ability to smooth out the airfoil as it sees fit. The downside to this method is that there would be practically double the amount of degrees of freedom, leading to a significantly longer optimization time. Another potential solution would be to remove the need for splines altogether. This would be done by significantly increasing the number of points along the upper and lower surface to create a relatively smooth curve. This would be the best solution, but the number of DoFs necessary would be on the order of 100-200, increasing the computational cost to nearly infeasible values.

One interesting discovery from the optimization was that the lift constraint was not active. This was contrary to what the team expected, as higher lift values generally cause shocks to form earlier which will increase their strength and the wave drag they create. This led to the idea that the minimum pressure on the upper surface of the airfoil should be constrained to prevent the airfoil's critical Mach number from being too low. By doing this, it can be assured the airfoil has a desired critical Mach number. In general, a transonic airfoil should have a critical Mach number that is approximately 0.05 lower than its design Mach number. For the current optimized airfoil, the minimum pressure coefficient on the upper surface is -1.18. Using Eq. 14 (Takahashi, 2014), the critical Mach

number can be calculated to be 0.706 for this airfoil, which is much lower than the desired value. Using Eq. 14, an objective minimum pressure can be calculated to be -0.987 to achieve a critical Mach number of 0.75. If this constraint is applied to the airfoil optimization, the problem may be better bounded and better results may be found that do not have an excess amount of lift.

$$C_P^{*\prime} = \frac{2}{\gamma \cos(\Lambda)\, M_\infty^2}\left(\left(\frac{2 + (\gamma - 1)M_\infty^2 \cos(\Lambda)^2}{\gamma + 1}\right)^{\frac{\gamma}{\gamma - 1}} - 1\right) \qquad (14)$$

One final improvement that could be made to the optimization method would be to modify what the optimizer is trying to vary to a find a minimum drag solution. Conventionally, an airfoil consists of two parts: a camber form and a thickness form. The camber form of an airfoil is the center of the airfoil, or the line down the center that is equidistant from the upper and lower surfaces. The thickness form is defined as the width of the airfoil at any given point along its camber line. In general, the thickness is added normal to the surface of the camber form to make the shape of the upper and lower surface of the airfoil. From a camber form and thickness form, the airfoil coordinates like those used in this optimization can be generated. But what is the benefit? Well, the trick is that the camber form and the thickness form each have their own unique effects on how the airfoil operates, and these effects are simply linearly superimposed onto each other (Donovan, 2014).

When doing the airfoil optimization, if the optimizer is varying the thickness form and camber form individually rather than the airfoil coordinates themselves, the gradient information will be more representative of the actual effects of changing camber and thickness. When varying the airfoil coordinates, these unique effects are lost so the optimization and response surface may perform worse. Varying camber and thickness form would also make sensitivity analysis and parametric studies significantly more meaningful to observers of the optimization. Interestingly, this method of defining an airfoil would have the same amount of degrees of freedom as the current methodology. This method of creating the airfoils was not implemented in this optimization project because it was realized much too late into the project to be implemented.

Because the aerodynamic optimization was a precursor to the other subsystems, it was practically independent from them. The only issue that could arise was if the optimizer tried to make the airfoil too thin so that the structural optimizations wouldn't work. After the fact, however, it seems that the geometric constraints applied to the airfoil geometry properly kept the airfoil from getting too thin, so

this was not an issue and the aerodynamic optimization was able to remain independent of the structural subsystem optimizations.

7.2. Modal Response

The results of the modal response subsystem optimization indicate that a universal spar thickness would not be the optimal solution. However, this may be the financially optimal solution in the real world as procuring multiple thicknesses, in multiple quantities, may be costly. The results make sense, though, since thicker sections of the interior have the greatest possibility for increasing the stiffness of the wing. For a simple rectangular section, the second moment of area increases as the cube of the height when bending about a central axis. This indicates that taller spars will be able to better increase the stiffness of the wing and decrease the resulting deflection under loading. This effect is easily seen in the optimal solution.

To further improve the solution, the model of the wing would need to include ribs along the span of the wing. These were left out of the optimization presented here for simplicity. Adding these in will likely have a significant effect on the optimal result. The overall weight of the wing will increase due to the increased material usage, and the stiffness at the locations of those ribs will be much higher than the stiffness between the ribs. Future optimization studies could take an approach similar to that presented here, where there are a fixed number of ribs at specified locations and each one is governed by a thickness constraint.

7.3. Deflection

The optimization results indicate that each spar is a different thickness. From a manufacturing standpoint, this greatly increases the complexity of the assembly process and the number of parts that need to be on-hand. From a design and structures standpoint, the different spar thicknesses are to be expected, because the stiffness required will depend on where the spar is located in the wing and what loads it will experience. The problem of varying thicknesses might be reduced or eliminated if additive manufacturing matures to the point where it can “print” part of the internal structure or even the entire wing. However, this is not likely to happen in the next few years. This means that a trade study will need to be done to compare what is optimal with what is acceptable and/or financially competitive.

8. System Integration Study

The three subsystems could not reasonably be optimized individually and then integrated at the end to find a system optimal design. This was largely due to the exterior shape of the airfoil being a controlling factor in how the internal structure would form. Therefore, an aerodynamically optimal design was found first, and then the internal structure was optimized within the bounds of the optimal external geometry.

As a result, the optimization of the airfoil did not share any optimization parameters with the other two subsystems. The output of the aerodynamics optimization was used as an input to the modal and deflection subsystems. These two subsystems shared the same geometry, which meant that they also shared the same set of optimization parameters. Those parameters were the constant skin thickness and the 16 spar thicknesses.

Figure 8-1 shows the setup used in ANSYS to perform the modal and deflection optimization. Even though two Response Surface Optimizations are shown, it was determined that the one titled "Full 2nd Order – MOGA" gave the best results in terms of prediction accuracy and overall results.

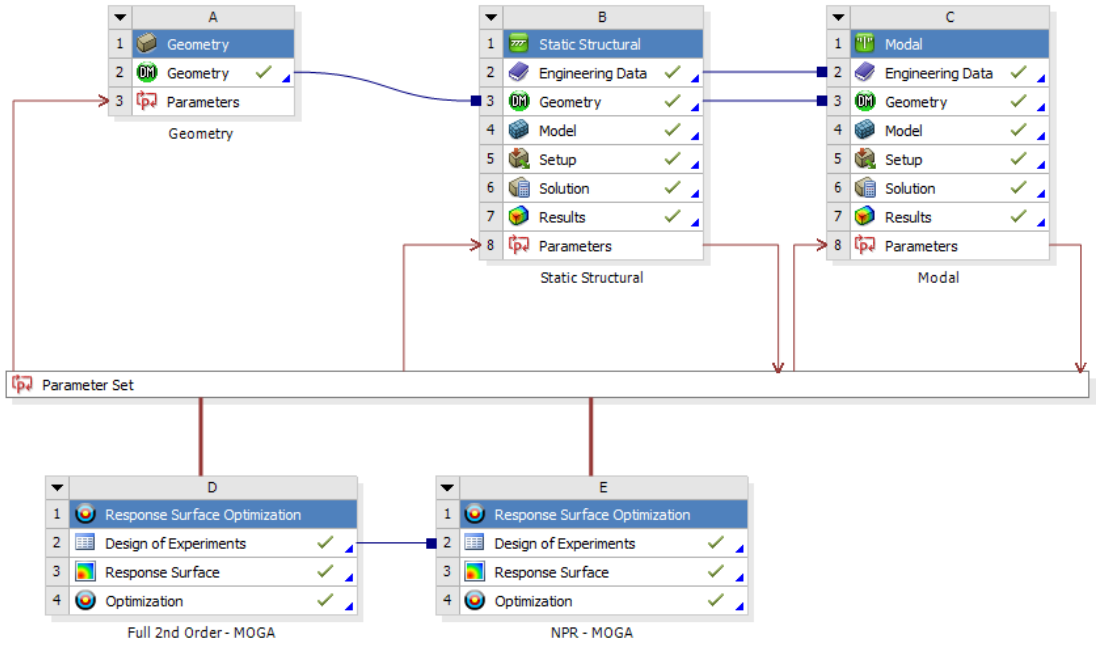

Figure 8-1 ANSYS Workbench Setup for Modal and Deflection Optimization

From the Response Surface Optimization, the 1st Pareto front can be shown in three plots to get an idea of how the objectives change with respect to one another. These are shown in Figure 8-2, Figure 8-3, and Figure 8-4 with linear and quadratic curve fits and their residuals.

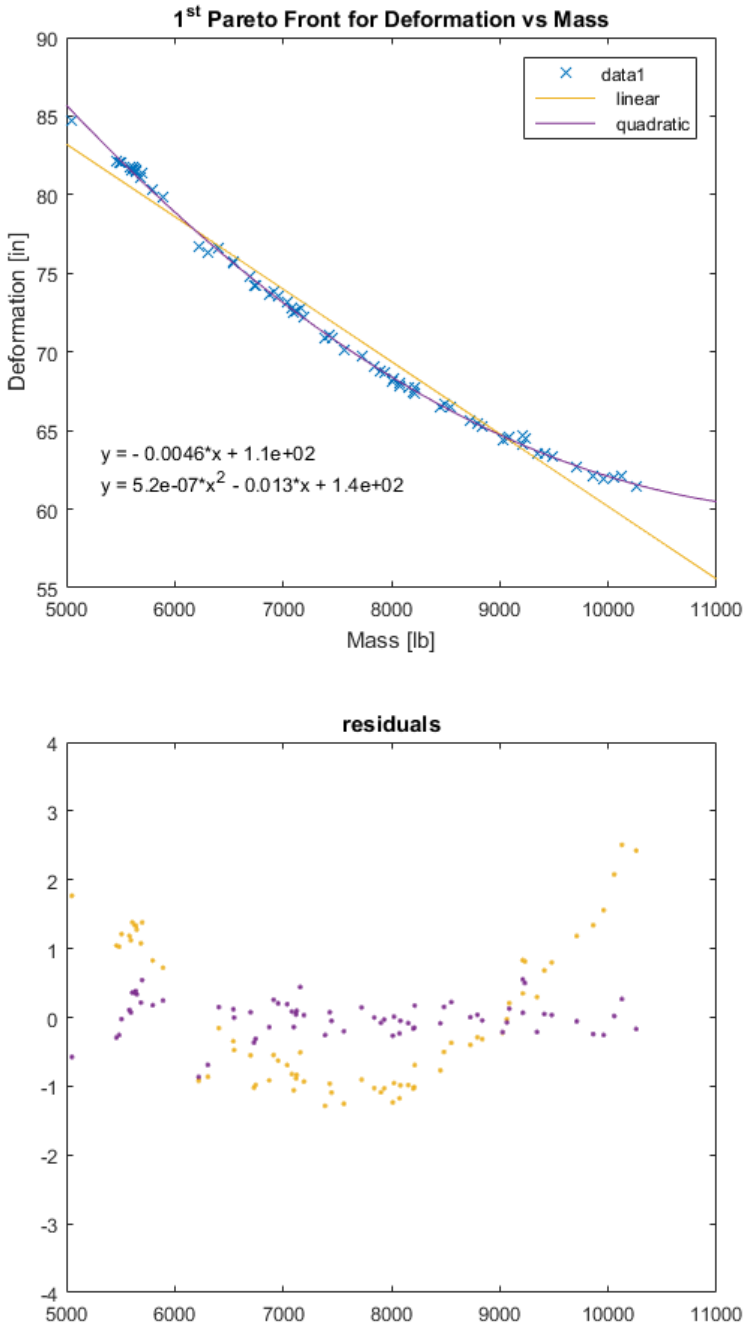

Figure 8-2 Pareto Front for Deformation vs. Mass

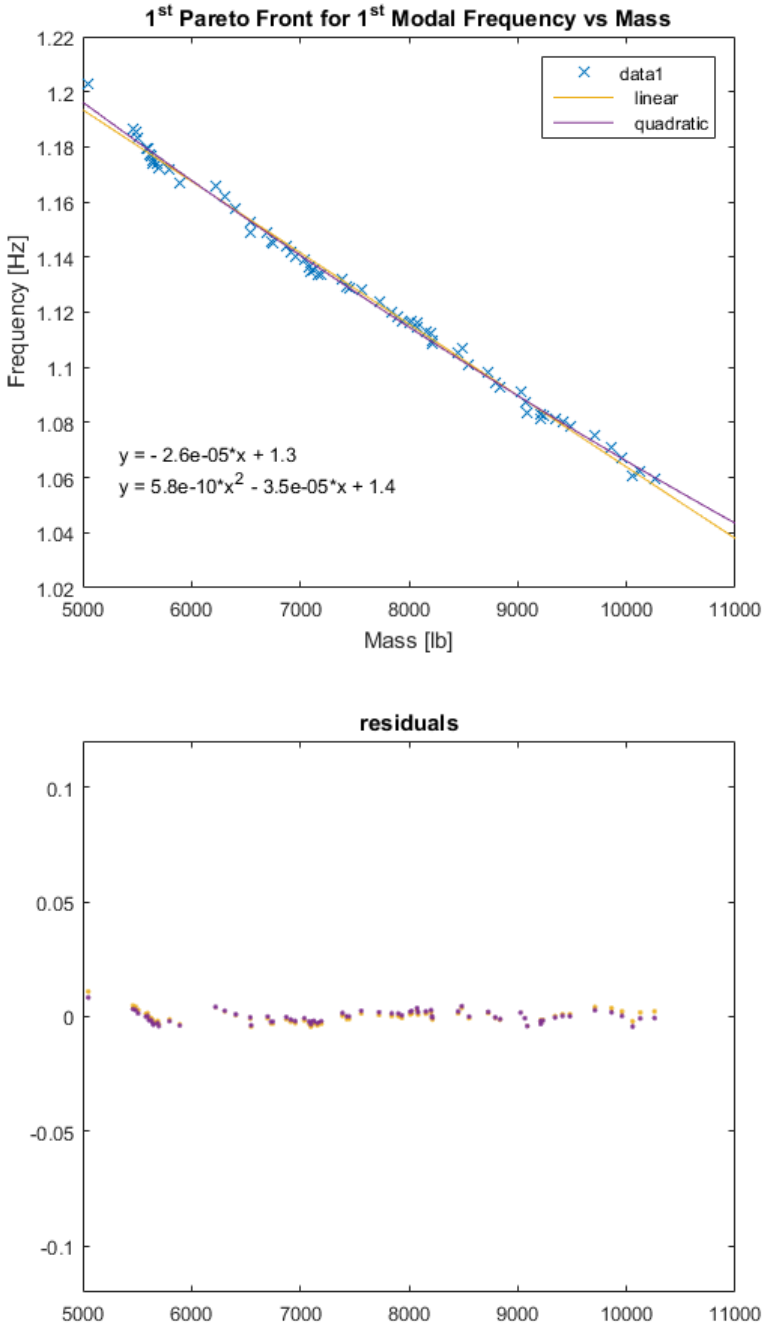

Figure 8-3 Pareto Front for Frequency vs. Mass

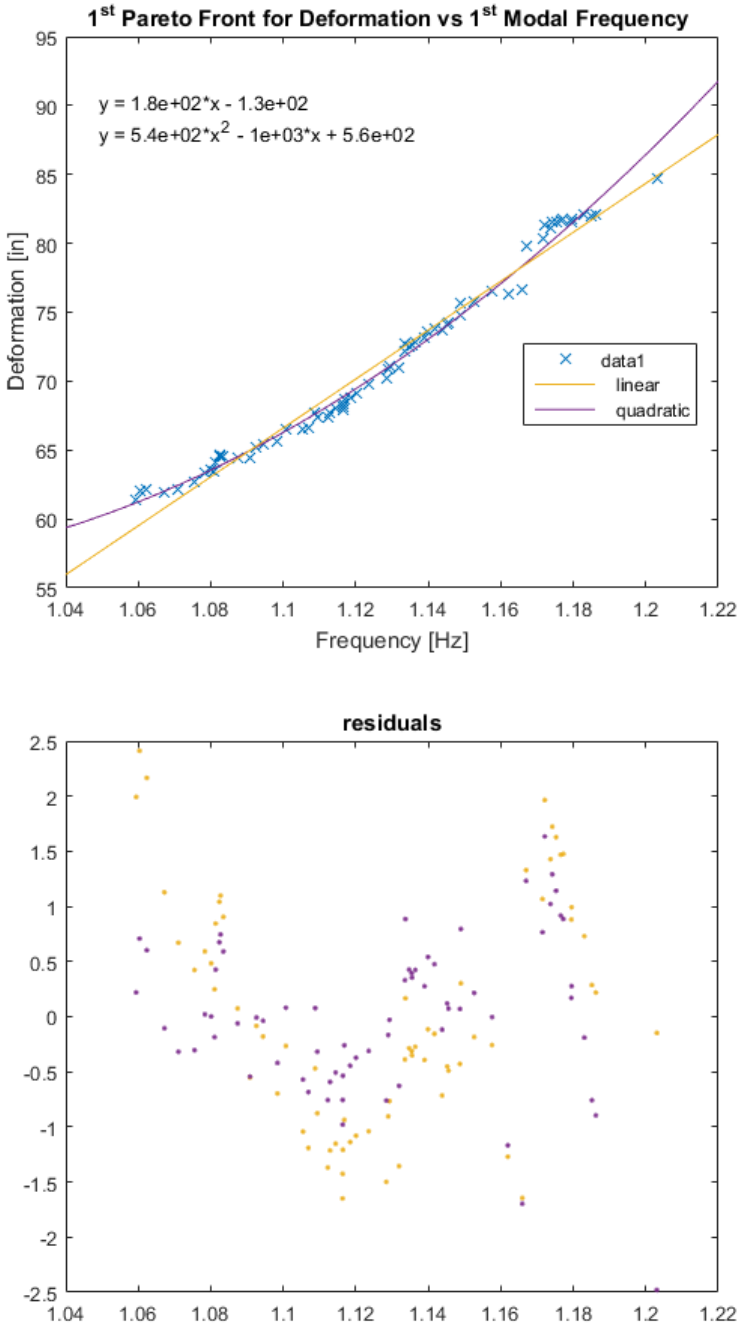

Figure 8-4 Pareto Front for Deformation vs. Frequency

From these Pareto fronts, a couple trends can be observed. From Figure 8-2 and Figure 8-4, a quadratic relationship is indicated not only by how well these curves fit the data, but also by the residuals. In Figure 8-2, the residuals of the linear fit show a parabolic-like pattern, indicating that a higher-order fit may be better suited to the data; this is also the case for Figure 8-4. Figure 8-3 shows that the relationship between the first modal frequency and the mass of structure is likely linear, and the quadratic fit does not show any obvious improvement.

These Pareto fronts also show the competing nature of the objectives for the modal and deflection optimizations. Figure 8-2 shows that the mass must increase in order to decrease the deflection, but Figure 8-3 shows that a lighter structure results in a higher first modal frequency. Furthermore, Figure 8-4 shows that a more flexible structure would result in a higher first modal frequency. This directly shows that the objectives of minimizing the deflection while maximizing the first modal frequency are, in fact, competing objectives.

9. References

[1] Anderson, J. D., “Modern Compressible Flow with Historical Perspective”, The McGraw-Hill Companies, New York, New York, 2003.

[2] Boyd, J. W., E. Migotsky and B. E. Wetzel. "A Study of Conical Camber For Triangular and Sweptback Wing." 1955.

[3] Donovan, S. M. and Takahashi, T. T., “A Rapid Synthesis Method to Develop Conceptual Design Transonic Wing Lofts”. Technical Paper. Tempe: Arizona State University, 2014.

[4] Drela, M., “Pros and Cons of Airfoil Optimization”, Frontiers of Computational Fluid Dynamics, 1998 D.A. Caughey, M.M. Hafez, Eds., World Scientific, ISBN 981-02-3707-3.

[5] Harris, Charles D. "NASA Supercritical Airfoils." Technical Paper. 1990.

[6] Herrin, D. W., “ANSYS Tutorial: Slides to Accompany Lectures in Vibro-Acoustic Design in Mechanical Systems”. Lexington, Kentucky, 2012. PDF.

[7] Kady, C.T., Dulin, D.J., and Takahashi, T.T., “A Method to Allocate Camber, Thickness and Incidence on a Swept Wing”, 2014.

[8] Mukhopadhyay, Vivek, “A Conceptual Wing Flutter Analysis Tool for Systems Analysis and Parametric Design Study”. Tech. NASA Langley Research Center. Web. 26 Jan. 2016.

[9] Pearcey, H. H. “The Aerodynamic Design of Section Shapes for Swept Wings”. Teddington, UK: National Physical Laboratory, 1958.

[10] Slater, J. W., “RAE 2822 Transonic Airfoil: Study #4” Glenn Research Center. URL: http://www.grc.nasa.gov/WWW/wind/valid/raetaf/raetaf04/raetaf04.html

10. Appendix A – RAE-2822 Coordinates and Image

RAE	2822	AIRFOIL									
Upper	Surface					Lower	Surface				
Xc	Zc	Xc	Zc	Xc	Zc	Xc	Zc	Xc	Zc	Xc	Zc
0	0	0.30866	0.059629	0.853553	0.026554	0	0	0.308658	-0.05846	0.853553	-0.00431
0.000602	0.003165	0.33156	0.06066	0.870476	0.023817	0.000602	-0.00316	0.331555	-0.05905	0.870476	-0.00283
0.002408	0.006306	0.35486	0.061497	0.886505	0.021153	0.002408	-0.00631	0.354858	-0.05924	0.886505	-0.00159
0.005412	0.009416	0.37851	0.062133	0.901604	0.01858	0.005412	-0.00944	0.37851	-0.05897	0.901604	-0.0006
0.009607	0.01248	0.40246	0.062562	0.915735	0.016113	0.009607	-0.01256	0.402455	-0.05822	0.915735	0.000157
0.014984	0.015489	0.42664	0.062779	0.928864	0.013769	0.014984	-0.01565	0.426635	-0.05698	0.928864	0.000694
0.02153	0.018441	0.45099	0.062774	0.940961	0.011562	0.02153	-0.01871	0.450991	-0.05526	0.940961	0.001033
0.029228	0.021348	0.47547	0.06253	0.951995	0.009508	0.029228	-0.02172	0.475466	-0.0531	0.951995	0.001197
0.03806	0.024219	0.5	0.062029	0.96194	0.007622	0.03806	-0.02469	0.5	-0.05056	0.96194	0.001212
0.048005	0.027062	0.52453	0.061254	0.970772	0.005915	0.048005	-0.02759	0.524534	-0.04772	0.970772	0.001112
0.059039	0.029874	0.54901	0.060194	0.97847	0.004401	0.059039	-0.03042	0.549009	-0.04464	0.97847	0.000935
0.071136	0.032644	0.57337	0.058845	0.985016	0.003092	0.071136	-0.03317	0.573365	-0.0414	0.985016	0.000719
0.084265	0.03536	0.59755	0.057218	0.990393	0.002001	0.084265	-0.03584	0.597545	-0.03804	0.990393	0.000497
0.098396	0.038011	0.62149	0.055344	0.994588	0.001137	0.098396	-0.03843	0.62149	-0.03463	0.994588	0.000296
0.113495	0.040585	0.64514	0.053258	0.997592	0.00051	0.113495	-0.04093	0.645142	-0.03121	0.997592	0.000137
0.129524	0.043071	0.66845	0.050993	0.999398	0.000128	0.129524	-0.04333	0.668445	-0.02781	0.999398	0.000035
0.146447	0.045457	0.69134	0.048575	1	0	0.146447	-0.04561	0.691342	-0.0245	1	0
0.164221	0.047729	0.71378	0.046029			0.164221	-0.04777	0.713778	-0.02129		
0.182803	0.049874	0.7357	0.043377			0.182803	-0.04981	0.735698	-0.01823		
0.20215	0.051885	0.75705	0.040641			0.20215	-0.05169	0.757051	-0.01536		
0.222215	0.053753	0.77779	0.037847			0.222215	-0.05343	0.777785	-0.01269		
0.242949	0.05547	0.79785	0.035017			0.242949	-0.05499	0.79785	-0.01024		
0.264302	0.057026	0.8172	0.032176			0.264302	-0.05638	0.817197	-0.00803		
0.286222	0.058414	0.83578	0.029347			0.286222	-0.05755	0.835779	-0.00605		

Figure 10-1 RAE-2822 Airfoil Coordinates (Slater, 2016)

Figure 10-2 RAE-2822 Airfoil

11. Appendix B – Aerodynamics Workbench Setup